Since January 2020 Elsevier has created a COVID-19 resource centre with free information in English and Mandarin on the novel coronavirus COVID-19. The COVID-19 resource centre is hosted on Elsevier Connect, the company's public news and information website.

Journal of Molecular Structure 1261 (2022) 132865

Contents lists available at ScienceDirect

Journal of Molecular Structure

journal homepage: www.elsevier.com/locate/molstr

New bis hydrazone: Synthesis, X-ray crystal structure, DFT computations, conformational study and *in silico* study of the inhibition activity of SARS-CoV-2

Abdelkader Tabbiche[a,b], Abdelaziz Bouchama[b], Nadjib Chafai[c,*], Farouk Zaidi[b], Chaabane Chiter[c], Messaoud Yahiaoui[c], Abdellah Abiza[a]

[a] *Laboratoire de Chimie, Ingénierie Moléculaire et Nanostructures, Université Ferhat Abbas Sétif 1, Sétif 19000, Algeria*
[b] *Département de chimie, Faculté des sciences, Université Ferhat Abbas-Sétif-1, Algeria*
[c] *Department of Process Engineering, Faculty of Technology, Laboratory of Electrochemistry of Molecular Materials and Complex (LEMMC). University of Ferhat ABBAS Setif-1, El-Mabouda campus, Sétif 19000, Algeria*

ARTICLE INFO

Article history:
Received 6 February 2022
Revised 16 March 2022
Accepted 17 March 2022
Available online 20 March 2022

Keywords:
Bis hydrazone
XRD
DFT
Conformational study
Molecular docking
COVID-19

ABSTRACT

The aim of this work was to synthesize new bis hydrazone derived from benzil in good yield, namely: (1Z,2Z)-1,2-bis (3-Chlorophenyl Hydrazino) Benzil, encoded by 3-Cl BHB. The benzil (or 1,2-diphenyl ethanedione) reacts with 3-Cl phenyl hydrazine by reflux method using ethanol as solvent to obtain the target compound. The obtained product is depicted by UV–Vis, IR spectroscopy and XRD-crystals analysis. All various contacts intra and intermolecular found in 3-Cl BHB were determined by the X-ray diffraction technique performed on single crystals. On the other hand, the optimized geometric structure of 3-Cl BHB was computed by the DFT/B3LYP method with 6–31 G (d, p) level. So, the bond lengths and angles, frontier molecular orbitals (FMO), surface electrostatic potential of the molecule (MEP), global reactivity descriptors, Mulliken atomic charges, computed vibrational analysis and electronic absorption spectrum were determined to get a good understanding of the electronic properties and the active sites of 3-Cl BHB, then to compare them with experimental data. Additionally, a conformational study was carried out using the same method (DFT). The structure-activity relationships established through molecular docking studies showed that 3-Cl BHB structure strongly binds to the receptors M^{pro} (-8.90 Kcal/mol) and RdRp (-8.60 Kcal/mol) which confirm its inhibition activity against COVID-19.

1. Introduction

COVID-19 is most common among older patients, particularly those with comorbidities such as diabetes, hypertension, obesity, and chronic kidney disease [1,2]. Despite significant progress in COVID-19 disease treatment tools, effective therapies for managing the novel coronavirus disease's long-term complications (COVID-19) are still lacking. COVID-19 is now found to affect other parts of the body in addition to the respiratory system [3]. In the meantime, the search for the appropriate vaccines and the effective drugs continues.

Due to the richness of many antiviral drugs on a significant number of nitrogen atoms and aromatic rings such as Merimepodib, Remdesivir and Mozenavir [4], we were motivated to synthesize a new bioactive compound of hydrazine derivatives called hydrazone. Because of its reaction efficiency and product stability, hydrazone formation, which is characterized by the formation of an $R_1R_2C{=}N{-}NH_2$ bond, stands out in medicinal and combinatorial chemistry as a promising method for intermolecular conjugation [5,6].

Generally, hydrazones are a special class of Schiff bases containing azomethine group (C = N) and N–N bound. So, they have been used as possible ligands for metal complexes in organic synthesis [7–10], optoelectronic applications [11,12] and organocatalysis [13]. Furthermore, due to their diverse pharmacological activities, hydrazone derivatives have recently attracted the attention of medicinal chemists. Many studies have found that these compounds have a wide range of biological activities, such as anticancer [14], antidiabetic [15], antioxidant [16], antimicrobial [17,18], antituberculosis [19], anticholinesterase [20], antifungal [21] and antiviral [22,23].

In the current work, novel bis-hydrazone was synthesized with a good yield. Single crystal X-ray diffraction (XRD), FT-IR, and UV–Vis spectroscopy were used to investigate the molecular structure and spectroscopic properties. As well, the Density Functional The-

* Corresponding author.
E-mail address: n.chafai@univ-setif.dz (N. Chafai).

https://doi.org/10.1016/j.molstruc.2022.132865
0022-2860/

ory (DFT) is used to gain a better understanding of the geometrical and electronic properties, then to compare them with the experimental data of the title compound. On the other hand, we wanted to see if the compound synthesized for the first time in this study could be antiviral agent candidate for use in the treatment of SARS-CoV-2 with an *in silico* study. Therefore, the molecular docking studies were carried out to know its interactions with the main protease (M^{pro}) and RNA dependent RNA polymerase (RdRp) of SARS-CoV-2.

2. Experimental section

2.1. Physical and material investigations

In this work, all the chemical reagents and solvents employed for the 3-Cl BHB ligand synthesis were available from commercial sources and used without any purification. The FT-IR in the range of 500–4000 cm^{-1} was recorded in solid state (KBr disks) using a Shimadzu FTIR-8010 M spectrometer. Electrothermal melting point apparatus was utilized for measuring melting point, and then the UV–Vis spectrum of the synthesized product was obtained in the range of 200–800 nm by UV–Vis 1800 UNICAM.

2.2. General procedure for the preparation of 3-Cl BHB

In a 100 ml flask, topped with a condenser, 1 g of benzil (4.76 mmol) is dissolved in 25 ml of ethanol and then mixed with this solution 1.36 g of 3-chlorophenylhydrazine (9.52 mmol), in order to speed up the reaction, a few drops of acetic acid were also added to the solution mixture. All were placed in the flask heater while stirring at a temperature of 80 °C for 7 h (Scheme 1), TLC was used to monitor the reaction until it was finished. At the end of the reaction and by cooling the reaction mixture, a light-yellow precipitate was obtained which was separated from the liquid phase by filtration (yellow 71%; m.p: 188 °C).The product was recrystallized by dimethylformamide (DMF).

2.3. X-ray diffraction and refining of single crystals

The diffracted intensities were set to 150 K on a Bruker-diffractometer. Nonius with Kappa geometry was equipped with a two-dimensional CCD type detector, (Nonius Kappa CCD diffractometer). The diffractometer was also equipped with a system cryoscopic with liquid nitrogen and a monochromator with a graphite blade according to the $\omega/2\theta$ scan, using the Kα radiation of Mo (λ = 0.71073 Å) at 150 K in a domain angular going from 2.93° to 27.48° The structures were solved by direct methods using the SHELXS-97 program and refined on F^2 by full matrix least squares [24]. Also, the crystalline structure was drawn using the Mercury and Ortep software [25,26]. The experimental data like the crystal system, conditions recording, mesh parameters, and others, are detailed in Table 1. Thus, copies of these information may be obtained free of charge from http://www.ccdc.cam.ac.uk or by emailing data_request@ccdc.cam.ac.uk, because the crystallographic data on the structure of 3-Cl BHB have been deposited in the Cambridge Crystallographic Data centre, with CCDC No: 2,101,205.

2.4. Computational methodology

Density functional theory (DFT) with Becke-3-Yang-Parr (B3LYP) hybrid parameter and standard basis sets 6–31 G (d, p) was used to calculate the optimized molecular structure of the title compound and their corresponding energies [27,28]. For a better study about our bis hydrazone and its active sites, bond lengths, bond angles, frontier molecular orbitals (FMO), surface electrostatic potential of the molecule (MEP), global reactivity descriptors and Mulliken atomic charges were carried out. The Gaussian 09 program package has been applied to perform all these calculations, while Gauss View was used for results visualizations and analysis [29,30]. Besides, the conformational analysis of synthesized compound has been investigated by this theory (DFT).

2.5. Molecular docking procedure

In this study, docking calculations of 3-Cl BHB ligand with SARS-CoV-2 main protease (M^{pro}) and RNA dependent RNA polymerase (RdRp) were used. They are generally used to predict the affinity of a ligand-protein and the most favorable position and orientation for a ligand interacting with a target protein. That is why, these simulations were performed by AutoDock software version 4.2.6, and a grid box size of 30Å × 30Å × 30Å centered at the pocket of protein at XYZ= (*−10.85, 12.58, 68.72*) was selected. In addition, the target proteins PDB structures were obtained from the RCSB protein data bank (Research Collaboratory for Structural Bioinformatics) with $M^{pro} \rightarrow$ *id* : 6LU7 and RdRp → id : 7BV2, the polar hydrogen atoms were added to the amino acid residues, while the water molecules were discarded and all of the protein's atoms were given Gasteiger charges [31]. The 3-Cl BHB-M^{pro} and 3-Cl BHB-RdRp complexes were visualized using Accelry's Discovery Studio Visualizer as represented in Fig. 1**a** and **b**, respectively.

3. Results and discussion

3.1. X-ray diffraction analysis

After a slow evaporation of our solution (3-Cl BHB in DMF), the structure and geometry of the obtained single crystals were analyzed by X-ray diffraction. This technique confirms exactly the molecular structure of the target compound. Fig. 2 shows the numbering scheme and a displacement ellipsoid plot of 3-Cl BHB, whereas the most important crystal properties are given in Table 1. Our bis-hydrazone crystallized in a triclinic system in P-1 space group and with a two molecules unit per cell (Z = 2) as displayed in Fig. 3.

The 3Cl-pH–HN–N = C_9_C_{29}=*N*–NH-pH-3Cl moieties were found to be in the s-Trans conformation, this positioning has been defined by the contact interactions and steric effects which forced a rotation of the two hydrazone units relative to C9-C29 single bond axis [32]. These two moieties are nearly perpendicular to one another by the dihedral angle $N_8C_9C_{29}N_{28}$ (−80.80°). On the other hand, the two phenyl rings of the benzil makes dihedral angles of −81.2°, which confirms that the geometry of the target compound is not planar. Furthermore, the azomethine groups were noted to be in Z configuration, which is involved in the torsion angles $N_7N_8C_9C_{10}$ [178.06(15)°] and $N_{27}N_{28}C_{29}C_{30}$ [178.60 (15)°]. Concerning bonds distances, the C = N bond lengths are 1.299 (2) Å for N_8=C_9 and 1.297 (2) Å for N_{28}=C_{29}, while the N–N (hydrazine) distance is in a typical single bond range [1.360(2)−1.357(2) Å]. Additionally, the C_1_Cl_1 andC_{21}_Cl_2 bonds distances are 1.748(19) and 1.744(2) Å, respectively, close to that expected for C–Cl bond (Table 4, Supplementary Information). All the results realized herein are similar to those found in the previous studies [33–35].

The atoms with a high electronegativity like Cl and N play a crucial role in most interactions; this is confirmed by the short contacts in our bis-hydrazone, which are summarized in two categories. The first is intramolecular contacts, depicted in Fig. 4**a** and Table 2**a**, where four interaction types are found π(C = N)….H_{Ph}(N8…H4, N8…H11, N28…H26 and N28…H31), two

(**a**)

(**b**)

Fig. 1. Best docked model visualization of the studied molecule with SARS-CoV-2 main protease (**a**) and RNA dependent RNA polymerase (**b**).

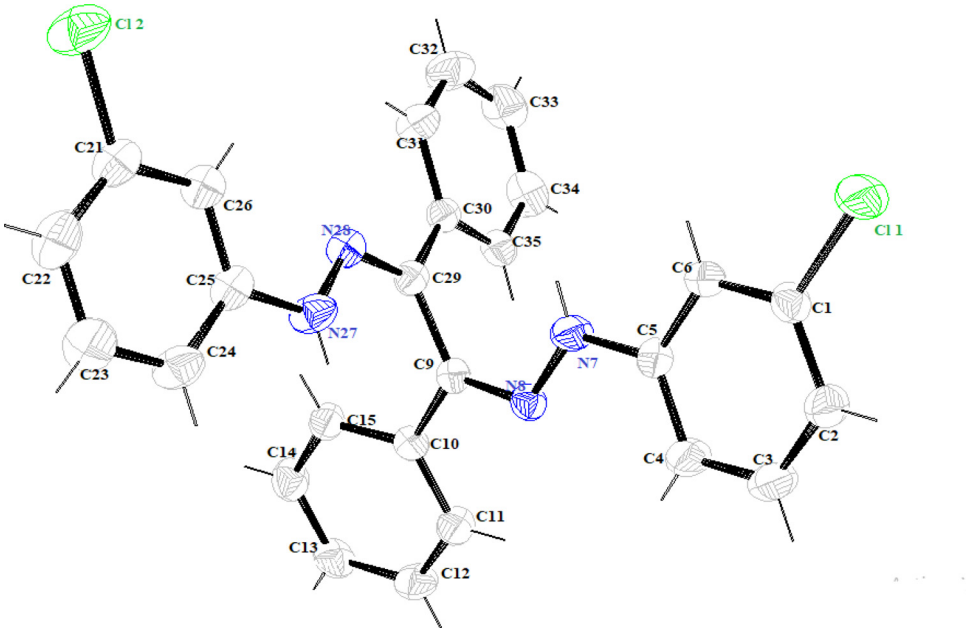

Fig. 2. 3-Cl BHB structure as seen by ORTEP at the 50% probability threshold, displacement ellipsoids are drawn.

Table 1
Crystallographic data and structure refinement detail for 3-Cl BHB.

Compound	**3-Cl BHB**
Empirical formula	$C_{26}H_{20}Cl_2N_4$
Formula weight, g/mol	459.36
Crystal system	Triclinic
Space group	P-1
Temperature/Ka (Å)	150(2)7.8551(5)
b (Å)	8.5174(5)
c (Å)	16.9720(13)
α (°)	77.943(3)
β (°)	86.730(3)
γ (°)	89.118(3)
V (Å^3)	1108.65(13)
Z	2
Crystal size/mm^{3}Data / restraints / parametersCalculated density (mg/mm^3)	0.3 × 0.22 × 0.174925 / 0 / 2951.376
Absorption coefficient(mm^{-1})Θ range for data collection (°)F (000)	0.3152.93 to 27.48476
Limiting indices(h,k,l)Absorption correction	$-8 \le h \le 10$, $-8 \le k \le 11$, $-21 \le l \le 21$Semi-empirical from equivalents
Max./min. trans.	0.948 and 0.864
Wavelength (Å)	0.71073
Reflections collected/ unique	13,443 / 4925[R(int) = 0.0507]
Refinement methodFinal R indices [I>2σ(I)]	Full-matrix least squares on $F^2$$R_1$=0.0498, wR_2 =0.1133
R indices (all data)S [Goodness of fit on F^2]	R_1 =0.0708, wR_2 =0.12271.083
Largest diff. peak/hole/e Å^{-3}	0.268 and −0.267

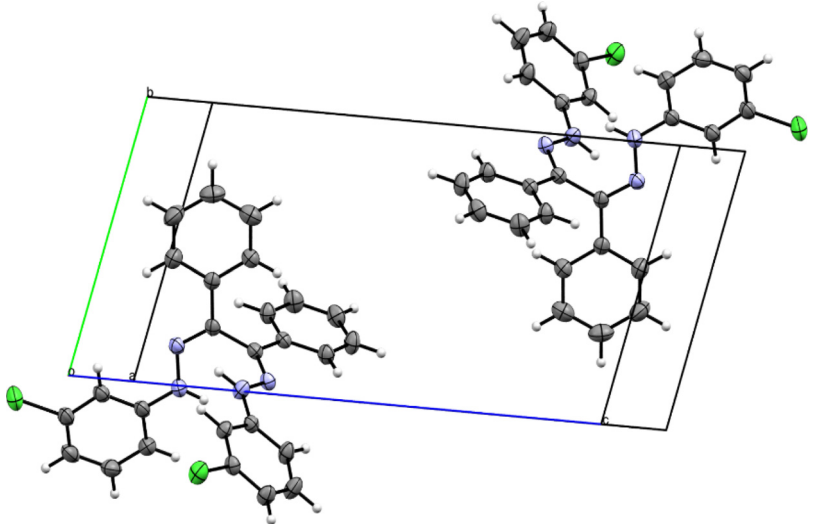

Fig. 3. Unit cell with the layered structure of the molecule in the crystal.

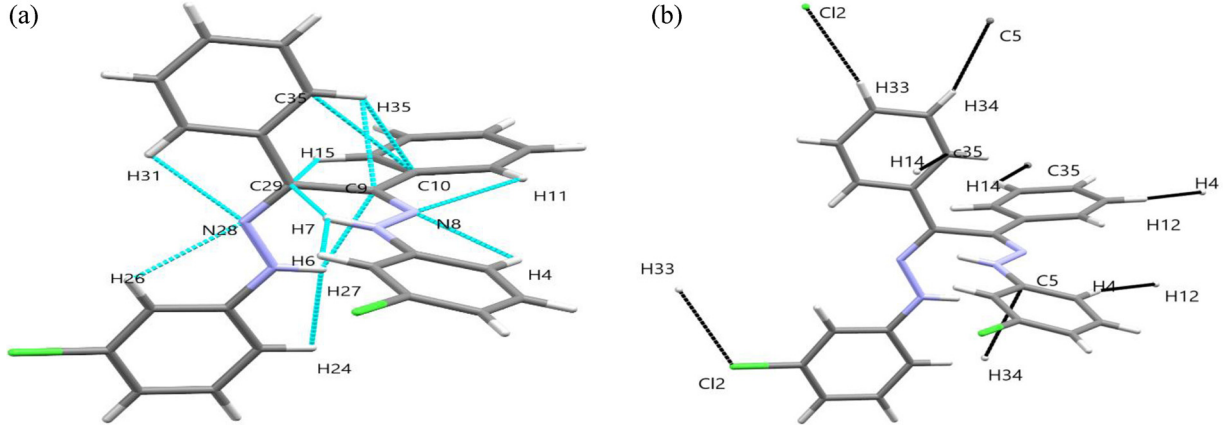

Fig. 4. **(a)**. Contact intramolecular in 3-Cl BHB. (**b).** Contact intermolecular in 3-Cl BHB.

Table 2
(a). Contact intramolecular.

Number	Atom1	Atom2	Length (Å)
1	H4	N8	2.518
2	H6	H7	2.361
3	H7	C29	2.354
4	N8	H11	2.562
5	C9	H27	2.366
6	C9	H35	2.509
7	C10	C35	3.351
8	C10	H35	2.747
9	H15	C29	2.526
10	H24	H27	2.346
11	H26	N28	2.549
12	N28	H31	2.561

(b). Contact intermolecular.

Number	Atom 1	Atom2	Length (Å)
12345678	C35H14C5H34Cl2H33H4H12	H14C35H34C5H33Cl2H12H4	2.8892.8892.7132.7132.9022.9022.3562.356

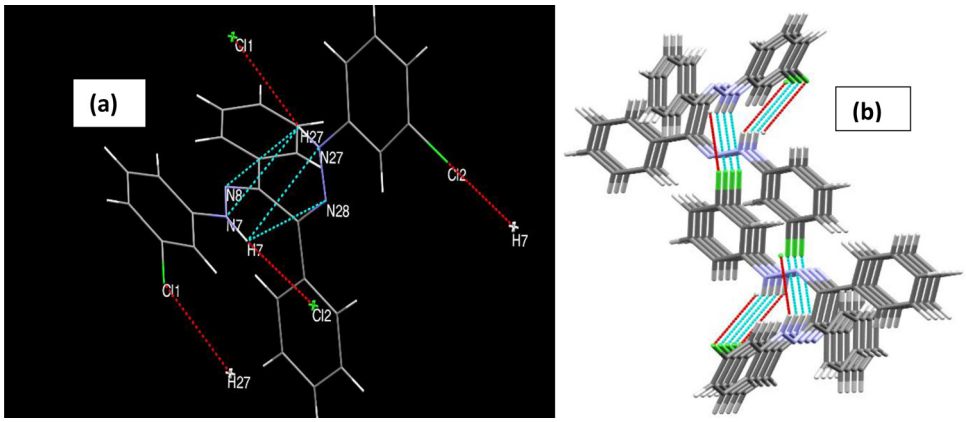

Fig. 5. **(a)**The hydrogen bonds (dashed lines), (**b**) a view along the a-axis in the crystal structure of 3-Cl BHB.

Table 3
3-Cl BHB H-bond angles (°) and distances (Å).

D-H ... A	d(D-H)	d(H ... A)	d(D-A)	D-H-A
Inter				
N7-H7...Cl2 ×2	0.889	3.215	4.029	153.28
N27-H27...Cl1 ×2	0.861	2.993	3.781	153.14
Intra	0.889	3.185	3.356	93.31
N7-H7...N27	0.889	2.783	3.231	112.60
N7-H7...N28	0.861	2.785	3.237	114.41
N27-H27...N8	0.861	3.166	3.356	95.22
N27-H27...N7				

corresponding N = C...HN (C9...H27, C29...H7) and others like H_{Ph}....π(pH) where they enhance the toughness of the compound. Concerning the second category called intermolecular contacts as represented in Fig. 4**b** and Table 2**b**, most of them were of the type H_{Ph}....π(pH) like (C5...H34 × 2 and C35...H14 × 2). Besides, there are a lot of H-bonds in the title product, which would control the conformation of 3-Cl BHB compound as mentioned earlier and make it more stable. Where N and Cl atoms acts as potent acceptor for H-bond in which atoms N7 and N27 donates a proton, as shown in Fig. 5**a** and Table 3. The crystal structure in 3-Cl BHB is oriented head to tail along the a-axis direction, in parallel columns driven by H-bonds (N–H...Cl) interactions, resulting in limitless chains, as seen in the Fig. 5**b**.

3.2. Computational analysis

3.2.1. Optimized molecular structure

To optimize the structure and establish key geometric parameters, the DFT approach was employed at the B3LYP level using the 6–31 G (d, p) basis set. The optimized molecular geometry (the most stable structures correlate to the lowest energy) of the 3-Cl BHB is shown in Fig. 6. Furthermore, the calculated total energy for this molecule in the best structure was −58,281.69 eV, which represents the energy of the more stable conformation of the analyzed ligand. The DFT gaseous state optimization revealed the 3-Cl BHB configuration with E-isomer in the two imine groups, rather than Z as in the crystalline structure. This is not surprising be-

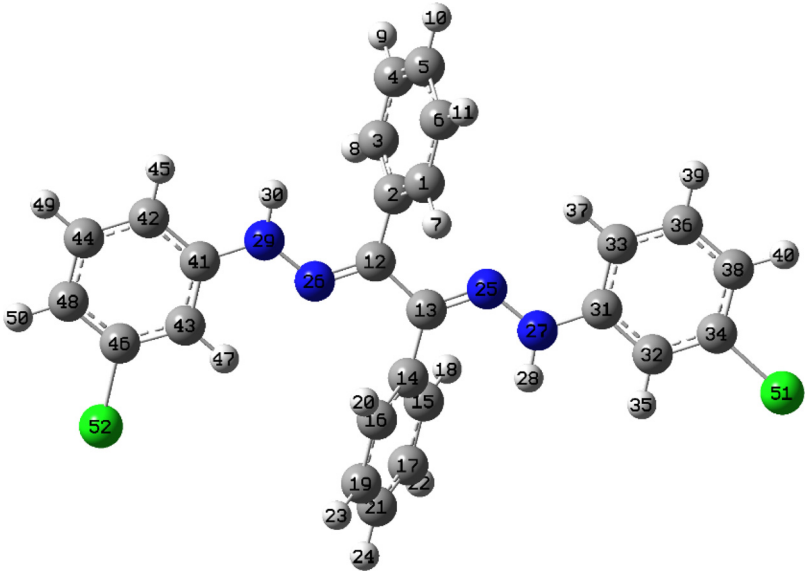

Fig. 6. Optimized structure of 3-Cl BHB.

Table 4
Selected bond distances (Å) and angles (°) from X-ray diffraction and DFT optimization for **3Cl-BHB.**

Bond lengths (Å)	Exp.	Calc.	Bond angles (°)	Exp.	Calc.
C1-Cl1	1.748(19)	1.832	**C6-C1-Cl1**	118.72(15)	118.21
C9-C10	1.474(2)	1.496	**C6-C5-N7**	118.08(17)	118.36
C9-C29	1.500(3)	1.466	**C6-C5-C4**	120.12(16)	119.88
C29-C30	1.475(3)	1.496	**C4-C5-N7**	121.76(17)	121.76
C5-N7	1.394(2)	1.397	**N8-N7-H7**	120.2(14)	120.18
N7-H7	0.89(2)	1.015	**C9-N8-N7**	116.96(16)	120.36
N7-N8	1.360(2)	1.358	**N8-C9-C10**	118.57(17)	123.63
N8-C9	1.299(2)	1.313	**N8-C9-C29**	122.20(16)	116.24
N27-N28	1.357(2)	1.358	**N28-C29-C9**	122.31(16)	116.39
N27-H27	0.86(2)	1.015	**C29-N28-N27**	117.46(16)	120.44
N28-C29	1.297(2)	1.312	**N28-N27-H27**	119.8(16)	120.29
C25-N27	1.399(2)	1.397	**C24-C25-N27**	118.18(18)	118.98
C21-Cl2	1.744(2)	1.832	**C26-C25-N27**	121.20(18)	121.09
C21-C26	1.390(3)	1.388	**C26-C21-Cl2**	118.47(17)	118.16
C30-C31	1.392(3)	1.407	**C29-C30-C35**	119.95(17)	120.14
C30-C35	1.394(3)	1.409	**C31-C30-C35**	118.31(18)	118.82

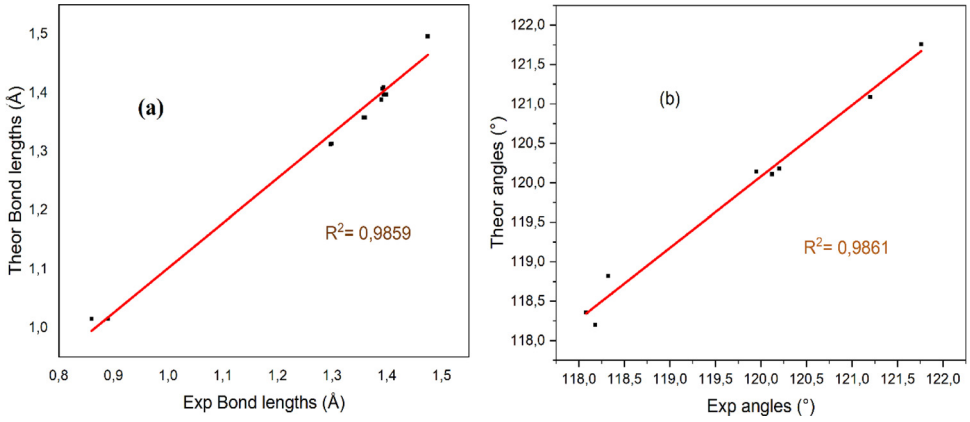

Fig. 7. DFT/XRD-graphical correlation for bond lengths **(a)** and bond angles **(b).**

cause in the gaseous state, E-isomers have a lower internal repulsion energy than Z-isomers [36]. Following this optimization, we conducted a comparison study with the XRD data. Table 4 lists the selected bond length (DRX/DFT) and bond angle (DRX/DFT) values, it was discovered that they are well matched, with correlation coefficients of R^2 = 0.9859 and 0.9861, respectively, as displayed in Fig. 7**a** and **b**.

3.2.2. Electronic properties and frontier molecular orbitals (FMO) analysis

The information regarding electrical and optical properties, as well as UV–Vis spectra and quantum chemistry, is provided by the frontier molecular orbital HOMO (Highest Occupied Molecular Orbital) and LUMO (Lowest Unoccupied Molecular Orbital), the gap between them, known as the orbital energy gap, is crucial in defin-

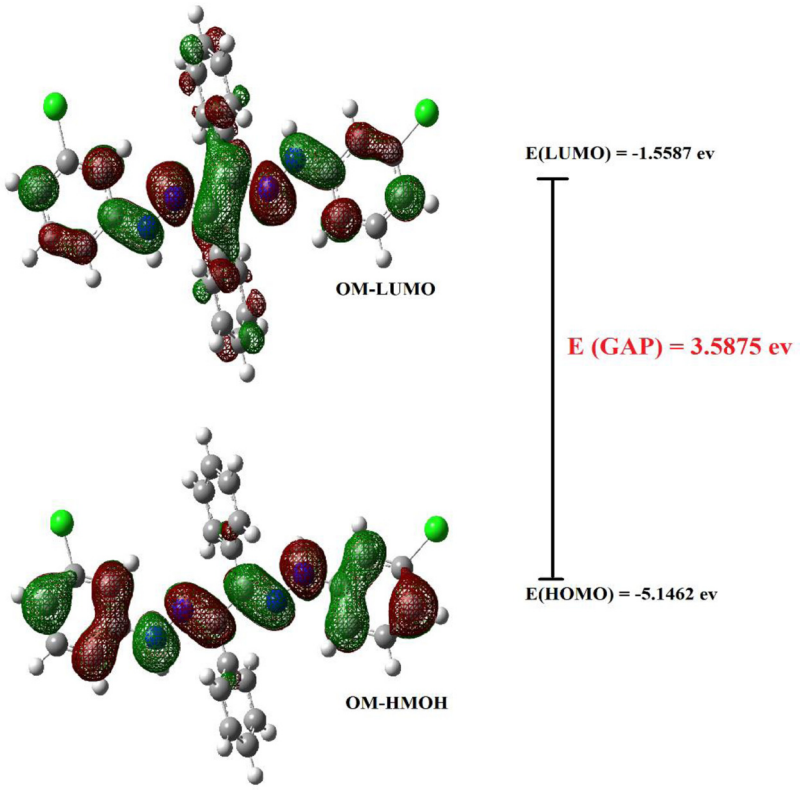

Fig. 8. HOMO and LUMO frontier orbitals of 3-Cl BHB.

Table 5
Calculated quantum chemical parameters of 3-Cl BHB using DFT/B3LYP 6–31 G (d,p) method.

Molecular energy (eV)	*3-Cl BHB*
E_{HOMO}	−5.1462
E_{LUMO}	−1.5587
Ionization Potential (I)	5.1462
Electron affinity (A)	1.5587
Chemical potential(μ)	−3.3525
Electronegativity (ϰ)	3.3525
Chemical hardness (η)	1.7938
Softness (S)	0.2787
Electrophilicity index (ω)	3.1328

$\boldsymbol{I} = -E_{HOMO}$, $\boldsymbol{A} = -E_{LUMO}$, $\mu = \frac{E_{HOMO}+E_{LUMO}}{2}$, $x = \frac{-(E_{LUMO}+E_{HOMO})}{2}$
$\omega = \frac{\mu^2}{2\eta}$, $S = \frac{1}{2\eta}$, $\eta = \frac{1}{2(E_{LUMO}-E_{HOMO})}$

ing the molecule's electron transport capability. A greater orbital energy gap indicates that the molecule is chemically hard, stable, and unreactive, whereas a lower orbital energy gap indicates that the molecule is soft, unstable, and reactive [37].

The quantum molecular descriptors of 3-Cl BHB such as ionization potential (I), electron affinity (A), global hardness (η), electronegativity (χ), electronic chemical potential (μ), electrophilicity (ω), and chemical softness (S) were calculated and summarized in Table 5 and they have helped in many ways to understand the structure of molecules and their reactivity. Ionization potential (I) and electron affinity (A) are the negative energies of HOMO and LUMO, respectively. The global hardness (η) corresponds to the energy gap between HOMO and LUMO. Also, the ability to give an electron orto accept an electron is represented by the HOMO and LUMO, respectively [38,39]. The ΔE_{Gap} value denotes the minimum amount of energy required for electronic excitation, which is mostly associated with the π-π^* transition [40].

At the B3LYP/ 6–31 G (d,p) level, the HOMO and LUMO in the stable conformer of 3-Cl BHB were determined and the 3D plots generated from the calculations are depicted in Fig. 8, their energies are equal to −5.1462 and −1.5587 eV, respectively. Therefore, ΔE_{Gap} value will be 3.5875 eV. In our compound, the HOMO is mainly focused over the two phenyl hydrazyl moieties; conversely the LUMO is projected over both of the molecule. There are two hues that stand out: green and red. Green indicates the negative phase, while red represents the positive phase. The query molecule's low energy gap (3.58 eV) indicates that it has higher chemical reactivity, lower dynamic stability, softness, and more polarizability, which means that the charge is easily transferred between the HOMO and LUMO orbitals of 3-Cl BHB [41]. We can divide organic compounds in to three categories based on their electrophilicity index values: marginal electrophiles with a value less than 0.8 eV, moderate electrophiles with a value between 0.8 and 1.5 eV, and strong electrophiles with a value greater than 1.5 eV [42]. Consequently, our bis-hydrazone will be strong electrophiles (3.13 eV). In the meantime, a nucleophilic attack on the 3-Cl BHB would be energetically advantageous and has good biological activity [43,44].

3.2.3. Surface electrostatic potential of the synthesized molecule (MEP)

The molecular electrostatic potential (MEP) is a three-dimensional map that depicts a molecule's charge distribution. It is a visual tool that can be used to determine the relative polarity of molecules and their negative and positive electrostatic potentials [45]. Generally, the MEP is used to gain a better understanding of active sites and to pinpoint the location of chemical reactivity in molecules. The colors scheme for the MEP of 3-Cl BHB is scaled from the deepest red maximum electron concentration ($-4.443\ 10^{-2}$ a.u.) to the deepest blue maximum electron deficient ($+4.443\ 10^{-}2$ a.u.) for 3-Cl BHB. Therefore, the MEP calcu-

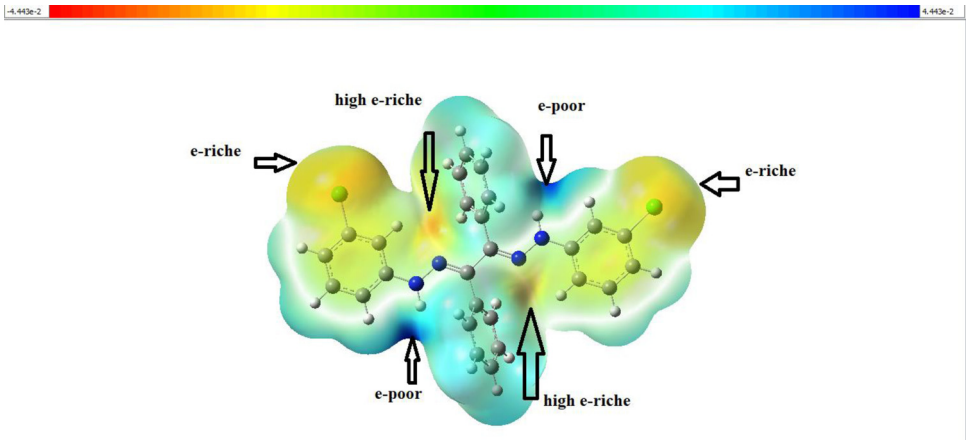

Fig. 9. Molecular electrostatic potential map of 3-Cl BHB.

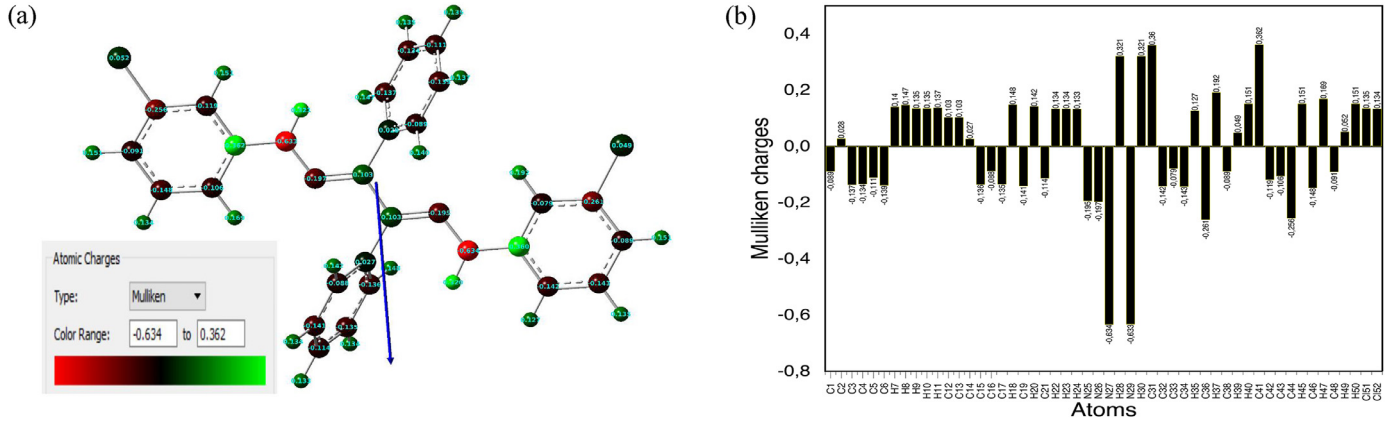

Fig. 10. (**a**). Mulliken atomic charges of 3-Cl BHB calculated at B3LYP/6–31 G (d,p) level. (**b**). The Mulliken atomic charge distribution of 3-Cl BHB.

lation surface of our compound as shown in Fig. 9, with different colors: the orange-colored high e-rich locations that covered the N of the imine functional group (nucleophilic site), then a relatively larger region around the chloro atoms of the phenyl hydrazyl, reflects by the yellowish blobs, represents e-riche locations (halogen with high electronegativity). On the other hand, the hydrogen atom of the NH group has the most positive potential region characterized by deep blue color (e-poor), corresponding to the nucleophilic reaction sites. Whereas the H atoms of aromatic rings found in zone blue sky carry positive charges. All of this is confirmed by the contacts intra and intermolecular present in our DRX analysis.

3.2.4. Analysis of the Mulliken atomic charges population

Many properties of molecular systems like dipole moment, polarizability, refractivity, and electronic structure are all influenced by the charge diffusion of donor and acceptor atoms in molecules [46]. For this purpose, the Milliken population charges were carried out through B3LYP/6–31 G (d, p) level and are presented in Fig. 10**a**, the bar diagrams of atomic charges are shown in Fig. 10**b.** Generally, the calculation revealed the presence of several atoms with nucleophilic and electrophilic properties. From this study, we found that both nitrogen atoms possess negative Mulliken charges. Furthermore, all carbon atoms have a negative charge except for the carbon atoms which are attached directly to the nitrogen atom (C12, C13, C31, C41). Concerning the H and Cl atoms are all electropositives, however the H atoms coupled to nitrogen atoms have larger positive atomic charges than the other hydrogen atoms (+0.320, +0.321 a.u) with high electrophilic properties indicate the ability to form H-bonds like as founded in our DRX analysis.

3.2.5. FT-IR analysis

For the purpose of confirming the expected formula and to discover the vibrational frequencies of the characteristic groups in our compound, it was depicted by IR analysis in the region of 500 and 4000 cm^{-1}. Fig. 11 shows the experimental and calculated IR spectra of 3-Cl BHB in which we find that our bis-hydrazone exhibit a new strong band assigned to azomethine υ(C = N) stretching vibration around 1597 cm^{-1} [47], besides one peak at higher wavenumbers (3420 cm^{-1}) is due to the stretching of the υ(N–H) vibrations. Concerning the $\upsilon(C–H_{Ar})$ stretching in the phenyl rings, it is located at 3311 cm^{-1} [48], while the strong absorption peaks at 1240, 1134 and 754 cm^{-1} are assigned to the stretching modes of υ(C–N), υ(N–N) and υ(C–Cl) [49], respectively. A good agreement has been obtained between DFT(B3LYP/6–31 G) and experimental spectra as noticed (Table 6), which means that the experimental values have a better correlation with the calculated values.

3.2.6. UV–Vis analysis

In order to have a better understanding of the electronic structure in the desired ligand, the experimental absorption behavior and TD-SCF CAM-B3LYP/6–31 G (d,p) computation were performed in the DMSO solvent, as shown in Fig. 12. The experimental spectrum of 3-Cl BHB showed two absorption bands, one located at λ_{max}= 299 nm and the other at λ_{max}= 392 nm, which may be attributed to $\pi \rightarrow \pi^*$ transition due to a conjugation in an unsaturated system and n $\rightarrow \pi^*$ excitation of the conjugation between the lone pair of electrons (N) and the others conjugated bond in 3-Cl BHB, respectively [50]. The absence of visible region absorption and the diversity of absorption peaks in the UV band ensure

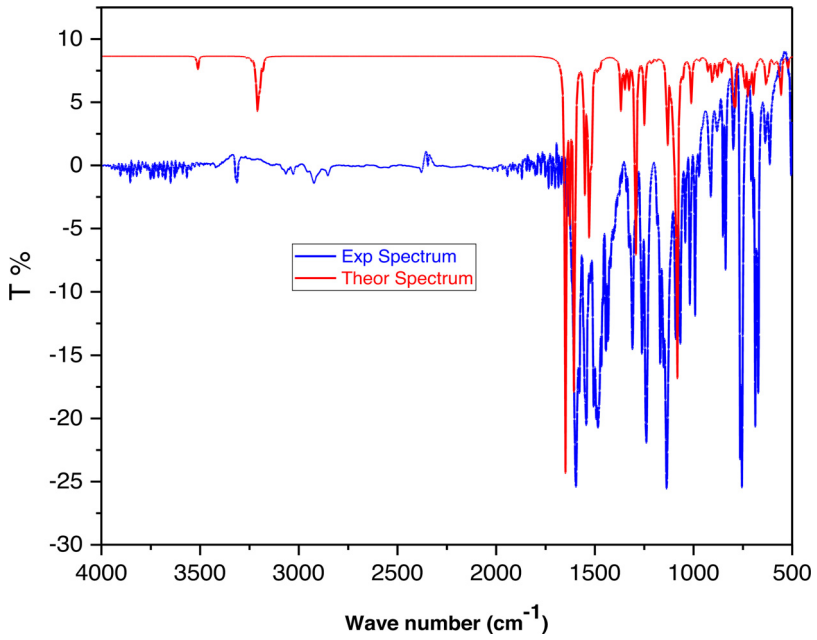

Fig. 11. Experimental and theoretical FT-IR spectra of 3-Cl BHB.

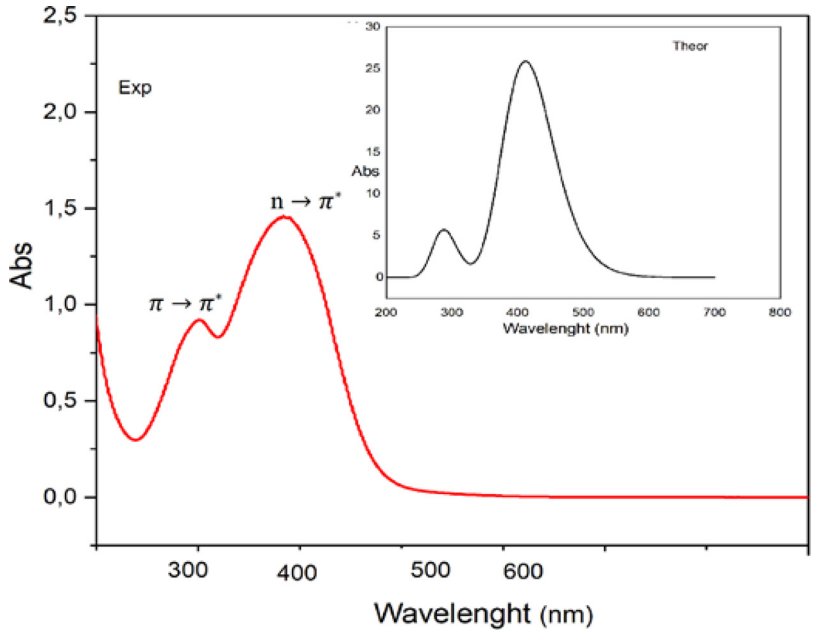

Fig. 12. Experimental and calculated electronic spectra (CAM-B3LYP) of 3-Cl BHB.

that the material is suitable for optical and photonic applications [51]. Conversely, the calculated spectrum founded through TD-SCF CAM-B3LYP/6–31 G (d,p) method for 3-Cl BHB compound showed a good resemblances in the shape and the band positions with the experimental UV–Vis spectrum in DMSO solvent. In which two broad peaks were detected by TD-DFT, the first is localized around 291 nm with $\Delta\lambda$= 8 nm shift, while the second peak at 401 nm due to HOMO→LUMO electron transfer which was in a good agreement with the n → π^* transition of the experimental UV–Vis spectrum ($\Delta\lambda$= 9 nm) [52].

3.2.7. Conformational study

According to the relative orientation of the two unsaturated bonds (C = N) around a single bond (C9–C29) in 3-Cl BHB compound predisposes the existence of several conformational isomeric structures. In order to obtain additional information on this stereochemical aspect, the potential energy surface (PES) for internal rotation around the N8-C9-C29-N28 dihedral angle was calculated using the B3LYP/6–31 G (d,p) level of approximation [53,54]. The PES was created by varying this dihedral angle from 0° to 180° with a step of 15° to determine the more stable conformer of our bis hydrazone. Fig. 13 shows the results of the PES scan for the selected dihedral angle. It seems that there are three conformers were detected: the least stable conformer namely s-*cis* is located at the point with the highest energy value of −58,281.97 eV, then another one has less energy than the first isomer at −58,282.03 eV corresponding to pseudo s-cis conformer, while the minimum energy conformation is attributed to an angle of −80° corresponding to s-trans form with relative energy value of −58,282.12 eV, we explain this more stable positioning by the intramolecular hydro-

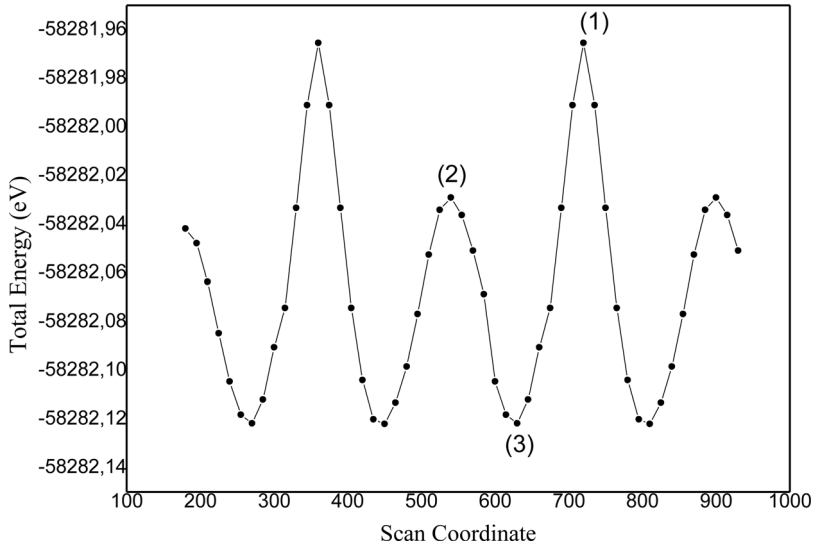

Fig. 13. Scan of total energy of N8-C9-C29-N28 dihedral angle calculated by B3LYP/6–31 G (d,p) method.

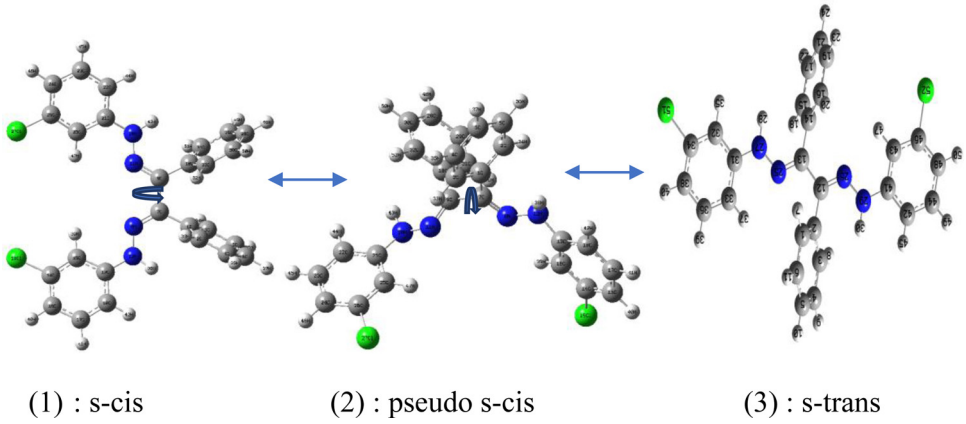

Fig. 14. Optimized structures of possible conformers of 3-Cl BHB.

Table 6
The calculated and experimental vibrational assignments of 3-Cl BHB.

Major Assignments	Exp wavenumbers (cm^{-1})	Calc wavenumbers (cm^{-1})
N-H stretching	3420	3501
vibration	3311	3209
C–H (aromatic)	2925	-
stretching	1597	1608
vibration	1534	1527
C–H (aliphatic)	1240	1283
stretching	1134	1086
vibration	754	780
C = N stretching		
vibration		
C = C in phenyl		
ring (stretching)		
C–N stretching		
vibration		
N–N (hydrazine)		
stretching		
vibration		
C–Cl stretching		
vibration		

gen bonds formed in 3-Cl BHB which we discovered through the DRX analysis [55], all of these conformers are depicted in Fig. 14. We observe that the molecular structure computed for the most stable conformer (s-trans) agrees very well with the structure experimentally determined from the single crystal X-ray diffraction analysis in solid state.

3.3. Molecular docking analysis

The molecular docking of 3-ClBHB ligand with the M^{pro} and RdRp receptors becomes completed to outline the precise conformation of the title compound in the receptor and the secondary forces resulting between 3-Cl BHB and the lively amino acids of the receptor.

3.3.1. SARS-CoV-2 main protease and 3-Cl BHB interaction

The detailed presentation of the binding modes of the studied molecule in the receptor M^{pro} as illustrated in Fig. 15**a**. With a view to this diagram, we observe that the title compound connects through van der Waals bond with the ASN142 amino acid, through Pi-sulfur interaction between the phenyl ring of the ligand and sulfur atom ofMET49 amino acid. In addition, it interacts through just one hydrogen bond with GLN189. Also, Pi-alkyl interactions are formed between Cl atoms in our bis hydrazone and LEU27, HIS41, HIS164 and MET165 amino acids residues of M^{pro}. All calculated lengths of these interactions are displayed in a 2D diagram, whereas the total binding energy of this complex is −8.90 Kcal/mol.

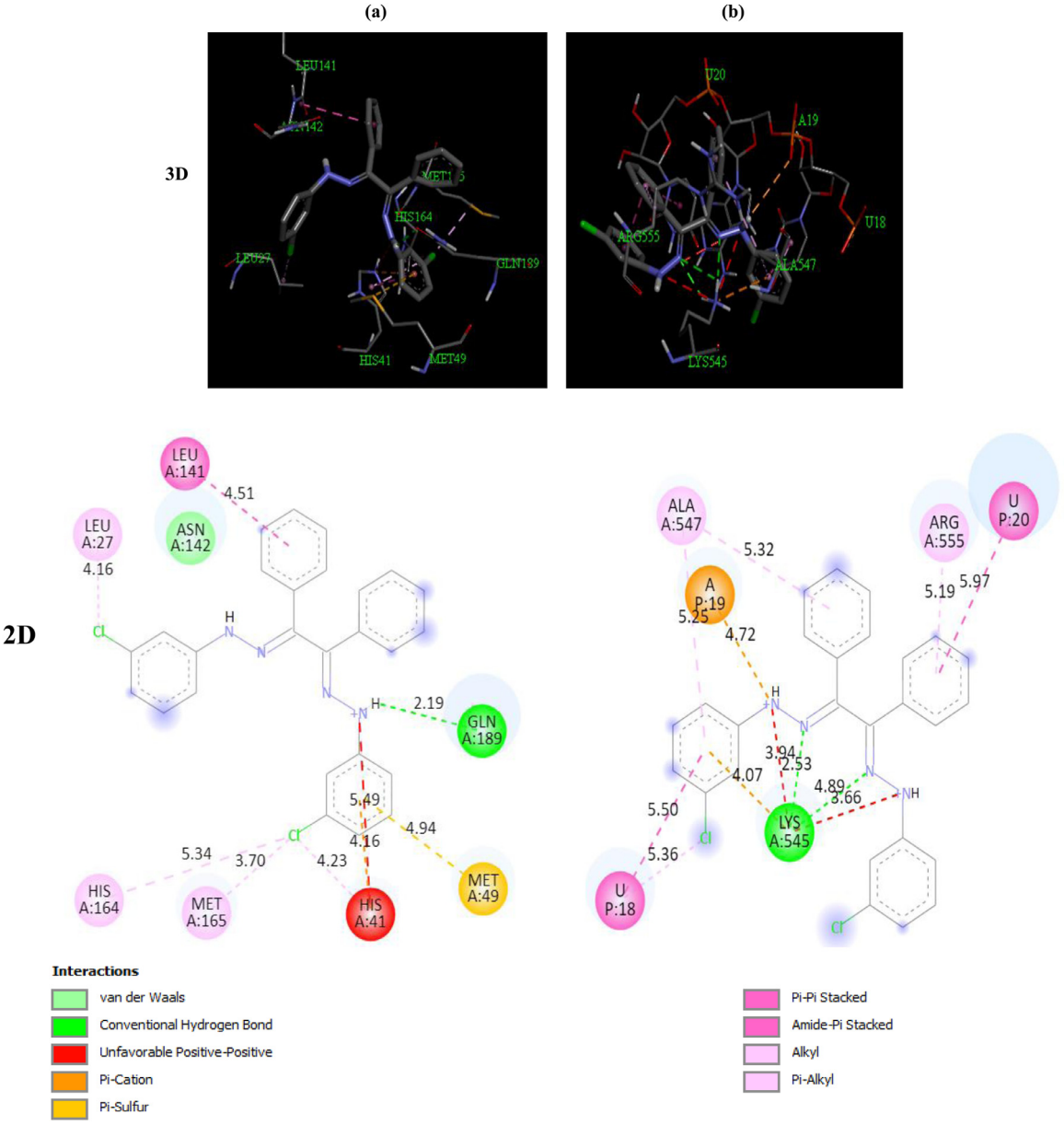

Fig. 15. 3D and 2D Binding-interaction diagrams of the studied molecule with SARS-CoV-2 main protease (**a**) and RNA dependent RNA polymerase (**b**).

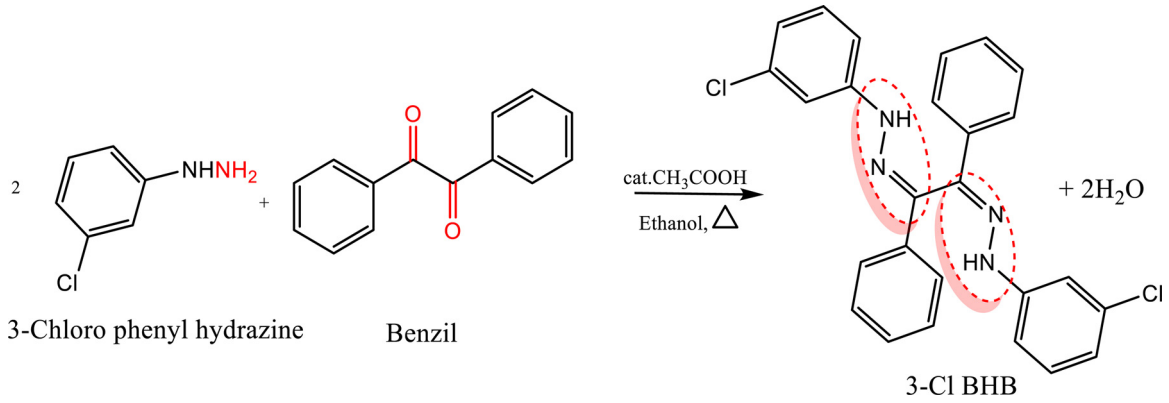

Scheme 1. The synthesis schematic for (1Z,2Z)−1,2-bis (3-Chlorophenyl Hydrazino) Benzil.

Table 7
Docking score results of 3–Cl BHB and some drugs with M^{pro} and RdRp.

Compounds	M^{pro} Binding energy in Kcal/mol	RdRp Binding energy in Kcal/mol
3-Cl BHB (the studied molecule)		
3-Cl BHB (the studied molecule)	−8.90	−8.60
	−6.00	−7.70
	− 6.5	−7.4
	−5.5	−5.6
	−5.7	−5.8
HDZPA		
HDZPA		
M1BZP		
M1BZP		
Hydroxychloroquine		
Hydroxychloroquine		
Moroxydine		
Moroxydine		

3.3.1. RNA dependent RNA polymerase and 3-Cl BHB interaction

Our present ligand has a good binding interaction with RdRp (−8.60 Kcal/mol). Fig. 15**b** represents the important interactions in the 3-Cl BHB-RdRp complex. According to the 2D diagram, we find that the 3-Cl BHB interacts with ALA547 and ARG555 by Pi-alkyl bonds, and then it was able to establish one Pi-cation interaction between A19 and N^+ of the title compound. In general, hydrogen bonds develop when hydrogen is bonded to a more electronegative atom, such as sulfur, nitrogen or oxygen, and another atom with a single pair of electrons [56], as illustrated in the case of our compound with the LYS545amino acid. Besides, the Pi-Pi stacking could be another hydrophobic interaction between the drug and the receptors, as in the aromatic rings of 3-Cl BHB with U20 and U18 nucleotides.

When we look at Table 7 which contains the values of binding energy of our molecule and other published inhibitors such as: HDZPA [57], M1BZP [58], Hydroxychloroquine [59] and moroxydine [4] with the same receptors. We find that these results give a clear view that 3-Cl BHB has the lowest values of the bending energy compared to the rest of the drugs, which confirms that our ligand have the stronger binding affinity towards M^{pro} and RdRp of SARS-CoV-2. This harmonious bonding may be due to the abundance of electron density (four aromatic rings, 2 atoms of Cl and 4 atoms of N) in 3-Cl BHB and the flexibility of its structure.

According to the findings of our research, we can consider 3-Cl-BHB as a potent inhibitor against corona virus and more effective along with other compounds having similar activity. However, there must be other studies and experiments on this compound to develop its activity.

4. Conclusion

We have successfully completed an efficient and convenient synthesis of new bis hydrazone derived from benzil in good yield, called (1Z,2Z)−1,2-bis (3-Chlorophenyl Hydrazino) Benzil and encoded by **3-Cl BHB**. UV–Vis, IR spectroscopy, and XRD-mono crystal were used to investigate the structure of the title compound. As well, DRX analysis enabled us to study the various contacts intra and intermolecular found in our bis hydrazone. Whereas, the Density Functional Theory (DFT) at the B3LYP/6–31 G (d,p) level was utilized to determine the active sites, electronic properties, quantum parameters and the most stable conformer of the examined molecule. Finally, after calculating the binding energies of M^{pro}-3-Cl BHB and RdRp-3-Cl BHB complexes by molecular docking and comparing it with other drugs having similar activity, we believe that our compound 3-Cl BHB can be a good inhibitor against SARS-CoV-2 main protease and RNA dependent RNA polymerase responsible for Coronavirus disease.

Declaration of Competing Interest

The authors declare that they have no known competing financial interests or personal relationships that could have appeared to influence the work reported in this paper.

CRediT authorship contribution statement

Abdelkader Tabbiche: Investigation, Formal analysis, Methodology, Software, Resources, Writing – original draft. **Abdelaziz Bouchama:** Conceptualization, Methodology, Validation. **Nadjib**

Chafai: Methodology, Software, Validation. **Farouk Zaidi:** Supervision. **Chaabane Chiter:** Supervision. **Messaoud Yahiaoui:** Supervision. **Abdellah Abiza:** Supervision.

Acknowledgement

This research was supported by the General Directorate for Scientific Research and Technological Development (DGRSDT), Algerian Ministry of Scientific Research, Laboratory of Electrochemistry of Molecular Materials and Complex (LEMMC), Ferhat ABBAS University of Setif.

References

[1] M. Covino, G. De Matteis, D.A.D. Polla, M. Santoro, M.L. Burzo, E. Torelli, B. Simeoni, A. Russo, C. Sandroni, A. Gasbarrini, F. Franceschi, Predictors of in-hospital mortality AND death RISK STRATIFICATION among COVID-19 PATIENTS aged >/= 80 YEARs OLD, Arch. Gerontol. Geriatr. 95 (2021) 104383.
[2] Q.Y. Peng, X.H. Ma, Z.Y. Liu, C.G. Zhao, L. Zhang, Z.X. Qian, L.N. Zhang, Differences in clinical characteristics between younger and older patients with COVID-19 and their relationship with the length of hospital stay, J. Intensive Med. 1 (2021) 123–129.
[3] E. Khani, S. Khiali, S. Beheshtirouy, T. Entezari-Maleki, Potential pharmacologic treatments for COVID-19 smell and taste loss: a comprehensive review, Eur. J. Pharmacol. 912 (2021) 174582.
[4] M. Mandal, S.K. Chowdhury, A.A. Khan, N. Baildya, T. Dutta, D. Misra, N.N. Ghosh, Inhibitory efficacy of RNA virus drugs against SARS-CoV-2 proteins: an extensive study, J. Mol. Struct. 1234 (2021) 130152.
[5] S. Rollas, S.G. Küçükgüzel, Biological activities of hydrazone derivatives, Molecules 12 (2007) 1910–1939.
[6] G. Rajmohan, R. Shanmugam, A. Elangovan, R. Sankaranarayanan, G. Ravindran, P. Dineshkumar, G. Arivazhagan, Synthesize, characterization and topological properties of new hydrazone derivatives, J. Mol. Struct. 1251 (2022) 132028.
[7] M. Maiti, S. Thakurta, G. Pilet, A. Bauzá, A. Frontera, Two new hydrogen-bonded supramolecular dioxo-molybdenum (VI) complexes based on acetyl-hydrazone ligands: synthesis, crystal structure and DFT studies, J. Mol. Struct. 1226 (2021) 129346.
[8] A. Thirugnanasundar, M.P. Kesavan, S.M. Kumar, L. Ravi, R. Bhaskar, G. Rajagopal, J. Rajesh, Synthesis, structure, DNA/protein molecular docking and biological studies of hydrazone ligand derived Cu (II) and VO (IV) complexes, Inorg. Chim Acta 526 (2021) 120543.
[9] S. Salah, Z.H. Abd El-Wahab, R.S. Farag, M.M. Mostafa, Synthesis, characterization and modeling structures of isatin-3-Girard T (IGT) and P (IGP) hydrazone complexes, Spectrochim. Acta Part A 124 (2014) 579–587.
[10] P. Sathyadevi, P. Krishnamoorthy, M. Alagesan, K. Thanigaimani, P.T. Muthiah, N. Dharmaraj, Synthesis, crystal structure, electrochemistry and studies on protein binding, antioxidant and biocidal activities of Ni (II) and Co (II) hydrazone complexes, Polyhedron 31 (2012) 294–306.
[11] R. Glaser, N. Knotts, P. Yu, L. Li, M. Chandrasekhar, C. Martin, C.L. Barnes, Perfect polar stacking of parallel beloamphiphile layers. Synthesis, structure and solid-state optical properties of the unsymmetrical acetophenone azine DCA, Dalton Trans. 23 (2006) 2891–2899.
[12] V. Meenatchi, S. Siva, L. Cheng, Synthesis, crystal growth, spectroscopic characterization, Hirshfeld surface analysis and DFT investigations of novel nonlinear optically active 4-benzoylpyridine-derived hydrazone, J. Mol. Struct. 1243 (2021) 130858.
[13] S. Vijayapritha, P. Viswanathamurthi, New half-sandwich (η6-p-cymene) ruthenium (II) complexes with benzothiazole hydrazone Schiff base ligand: synthesis, structural characterization and catalysis in transamidation of carboxamide with primary amines, J. Organomet. Chem. 929 (2020) 121555.
[14] R. Çakmak, E. Başaran, S. Kaya, S. Erkan, Synthesis, spectral characterization, chemical reactivity and anticancer behaviors of some novel hydrazone derivatives: experimental and theoretical insights, J. Mol. Struct. 1253 (2021) 132224.
[15] G. Yapar, H.E. Duran, N. Lolak, S. Akocak, C. Türkeş, M. Durgun, M. Işık, Ş. Beydemir, Biological effects of bis-hydrazone compounds bearing isovanillin moiety on the aldose reductase, Bioorg. Chem. 117 (2021) 105473.
[16] I. Mhaidat, F. Alwedian, T. Ababneh, A. Shdefat, H. Tashtoush, Synthesis, characterization, computational, antioxidant and fluorescence properties of novel 1, 3, 5-trimesic hydrazones derivatives, Heliyon 7 (2021) e08074.
[17] M. Krátký, K. Konečná, M. Brablíková, J. Janoušek, V. Pflégr, J. Maixnerová, F. Trejtnar, J. Vinšová, Iodinated 1, 2-diacylhydrazines, benzohydrazide-hydrazones and their analogues as dual antimicrobial and cytotoxic agents, Bioorg. Med. Chem. 41 (2021) 116209.
[18] A. Cukurovali, E. Yilmaz, Synthesis, characterization, investigation of biological activity and theoretical studies of hydrazone compounds containing choloroacetyl group, J. Mol. Struct. 1075 (2014) 566–578.
[19] F.R. Pavan, P.I.D.S. Maia, S.R. Leite, V.M. Deflon, A.A. Batista, D.N. Sato, S.G. Franzblau, C.Q. Leite, Thiosemicarbazones, semicarbazones, dithiocarbazates and hydrazide/hydrazones: anti–Mycobacterium tuberculosis activity and cytotoxicity, Eur. J. Med. Chem. 45 (2010) 1898–1905.
[20] M. Bingul, S. Ercan, M. Boga, The design of novel 4, 6-dimethoxyindole based hydrazide-hydrazones: molecular modeling, synthesis and anticholinesterase activity, J. Mol. Struct. 1213 (2020) 128202.
[21] G. Turan-Zitouni, M.D. Altıntop, A. Özdemir, F. Demirci, U.A. Mohsen, Z.A. Kaplancıklı, Synthesis and antifungal activity of new hydrazide derivatives, J. Enzyme Inhib. Med. Chem. 28 (2013) 1211–1216.
[22] O.I. El-Sabbagh, H.M. Rady, Synthesis of new acridines and hydrazones derived from cyclic β-diketone for cytotoxic and antiviral evaluation, Eur. J. Med. Chem. 44 (2009) 3680–3686.
[23] T. Topal, Y. Zorlu, N. Karapınar, Synthesis, X-ray crystal structure, IR and Raman spectroscopic analysis, quantum chemical computational and molecular docking studies on hydrazone-pyridine compound: as an insight into the inhibitor capacity of main protease of SARS-CoV2, J. Mol. Struct. 1239 (2021) 130514.
[24] G. Sheldrick, in: SHELXL-97. Programs for Crystal Structure Analysis, 4, University of Gottingen, 1998, p. 3400. Release 97-2.
[25] C.F. Macrae, P.R. Edgington, P. McCabe, E. Pidcock, G.P. Shields, R. Taylor, M. Towler, J. Streek, Mercury: visualization and analysis of crystal structures, J. Appl. Crystallogr. 39 (2006) 453–457.
[26] L. Farrugia, ORTEP 3 for Windows, Version 1.0. 1β, University of Glasgow, 1997; LJ Farrugia, J. Appl. Crystallogr 30 (1997) 565.
[27] T. Lohith, S. Shamanth, M. Sridhar, K. Mantelingu, N. Lokanath, Synthesis, molecular structure, Hirshfeld surface, energy framework and DFT studies of 1, 3, 4 oxadiazole derivative, J. Mol. Struct. 1252 (2021) 132203.
[28] F. Mostaghni, A. Teimouri, S.A. Mirshokraei, Synthesis, spectroscopic characterization and DFT calculations of β-O-4 type lignin model compounds, Spectrochim. Acta Part A 110 (2013) 430–436.
[29] B.K.R.M. Krishna Priya, V. Renuka, S. Sathya, P. Samuel Asirvatham, in: Molecular structure, spectroscopic (FT-IR, FT-Raman, 13C and 1H NMR) analysis, HOMO-LUMO energies, mulliken, MEP and thermal properties of new chalcone derivative by DFT calculation, 8, 2019, pp. 37–46.
[30] Y. Zhu, C.K. Xia, S.C. Meng, J. Chen, J. Chen, J.M. Xie, Syntheses, structures, properties and DFT calculations of coordination polymers constructed by 2, 6-bis (benzimidazolyl) pyridine, Polyhedron 61 (2013) 181–187.
[31] M. Hagar, H.A. Ahmed, G. Aljohani, O.A. Alhaddad, Investigation of some antiviral N-heterocycles as COVID 19 drug: molecular docking and DFT calculations, Int. J. Mol. Sci. 21 (2020) 3922.
[32] G. Elmacı, H. Duyar, B. Aydıner, I. Yahaya, N. Seferoğlu, E. Şahin, S.P. Çelik, L. Açık, Z. Seferoğlu, Novel benzildihydrazone based Schiff bases: syntheses, characterization, thermal properties, theoretical DFT calculations and biological activity studies, J. Mol. Struct. 1184 (2019) 271–280.
[33] P. Sivajeyanthi, M. Jeevaraj, B. Edison, K. Balasubramani, Crystal structure and Hirshfeld surface analysis of (E)-2-(5-bromo-2-hydroxybenzylidene) hydrazinecarbothioamide dimethyl sulfoxide monosolvate, Acta Crystallogr. Sect. E Crystallogr. Commun. 74 (2018) 119–123.
[34] N. Ghichi, C. Bensouici, A. Benboudiaf, Y. DJebli, H. Merazig, Crystal structures and antioxidant capacity of (E)-5-benzyloxy-2-{[(4-chlorophenyl) imino] methyl} phenol and (E)-5-benzyloxy-2-({[2-(1H-indol-3-yl) ethyl] iminiumyl} methyl) phenolate, Acta Crystallogr. Sect. E Crystallogr. Commun. 74 (2018) 478–482.
[35] G. Elmacı, E. Aktan, N. Seferoğlu, T. Hökelek, Z. Seferoğlu, Synthesis, molecular structure and computational study of (Z)-2-((E)-4-nitrobenzylidene) hydrazone)-1, 2-diphenylethan-1-one, J. Mol. Struct. 1099 (2015) 83–91.
[36] A. AlObaid, M. Suleiman, C. Jama, A. Zarrouk, I. Warad, Synthesis, physicochemical, optical, thermal and TD-DFT of (E)-N′-((9-ethyl-9H-carbazol-3-yl)-methylene)-4-methyl-benzene-sulfonohydrazide (ECMMBSH): naked eye and colorimetric Cu^{2+} ion chemosensor, J. King Saud Univ. Sci. 33 (2021) 101633.
[37] F.H. Al-Ostoot, D.V. Geetha, Y.H.E. Mohammed, P. Akhileshwari, M.A. Sridhar, S.A. Khanum, Design-based synthesis, molecular docking analysis of an anti-inflammatory drug, and geometrical optimization and interaction energy studies of an indole acetamide derivative, J. Mol. Struct. 1202 (2020) 127244.
[38] S. Masoome, S. Shahab, R. Alnajjar, M. Ahmadianarog, Theoretical model for surface forces between cytosine and CNT(6,6-6) nanotube: geometry optimization, molecular structure, intermolecular hydrogen bond, spectroscopic (NMR, UV/Vis, excited state), FMO, MEP, and HOMO–LUMO investigations, Russ. J. Phys. Chem. A 93 (2019) 2429–2443.
[39] Y. Umar, S. Abdalla, DFT study of the molecular structure, conformational preference, HOMO, LUMO, and vibrational analysis of 2-, and 3-furoyl chloride, J. Solut. Chem. 46 (2017) 741–758.
[40] Y.N. Mabkhot, F.D. Aldawsari, S.S. Al-Showiman, A. Barakat, S.M. Soliman, M.I. Choudhary, S. Yousuf, M.S. Mubarak, T.B. Hadda, Novel enaminone derived from thieno [2,3-b] thiene: synthesis, X-ray crystal structure, HOMO, LUMO, NBO analyses and biological activity, Chem. Cent. J. 9 (2015) 1–11.
[41] S. Şahin, N. Dege, Synthesis, characterization, X-ray, HOMO-LUMO, MEP, FT-IR, NLO, hirshfeld surface, ADMET, boiled-egg model properties and molecular docking studies with human cyclophilin D (CypD) of a Schiff base compound:(E)-1-(5-nitro-2-(piperidin-1-yl) phenyl)-N-(3-nitrophenyl) methanimine, Polyhedron 205 (2021) 115320.
[42] M.J.A. Luis, R. Domingo, P. Pérez, R. Contreras, Qantitative characterization of the global electrophilicity power of common diene/dienophile pairs in Diels-alder reactions, Tetrahedron 58 (2002) 4417–4423.
[43] A. Saral, P. Sudha, S. Muthu, B. Rajaraman, S. Selvakumari, P. Sangeetha, Quantum mechanical, spectroscopic vibrational analysis, NBO, HOMO-LUMO, and molecular docking studies on 2-Chloroquinoline-3-Carboxamide, Materialstoday Proc. (2020).
[44] J.C. Jebapriya, J.C. Prasana, S. Muthu, B.F. Rizwana, in: Spectroscopic (FT-IR and FT-Raman), quantum computational (DFT) and molecular docking studies on 2 (E)-(4-N, N-dimethylaminobenzylidene)-5-methylcyclohexanone, 2020.

[45] B.K. Shukla, U. Yadava, in: DFT calculations on molecular structure, MEP and HOMO-LUMO study of 3-phenyl-1-(methyl-sulfonyl)-1H-pyrazolo [3,4-d]pyrimidine-4-amine, 49, 2022, pp. 3056–3060.
[46] S. Mugeshini, R. Santhakumari, N. Rajeswari, G. Amudha, D. Chandrika, S. Sagadevan, Growth and computational studies on vanillin isoniazid single crystals, Chin. J. Phys. 72 (2021) 229–239.
[47] Y. Kaya, C. Icsel, V.T. Yilmaz, O. Buyukgungor, A palladium(II) complex containing both carbonyl and imine oxime ligands: crystal structure, experimental and theoretical UV-vis, IR and NMR studies, Spectrochim. Acta A Mol. Biomol. Spectrosc. 108 (2013) 133–140.
[48] S. Naseem, M. Khalid, M.N. Tahir, M.A. Halim, A.A. Braga, M.M. Naseer, Z. Shafiq, Synthesis, structural, DFT studies, docking and antibacterial activity of a xanthene based hydrazone ligand, J. Mol. Struct. 1143 (2017) 235–244.
[49] M. Arshad, K. Ahmed, M. Bashir, N. Kosar, M. Kanwal, M. Ahmed, H.U. Khan, S. Khan, A. Rauf, A. Waseem, T. Mahmood, Synthesis, structural properties and potent bioactivities supported by molecular docking and DFT studies of new hydrazones derived from 5-chloroisatin and 2-thiophenecarboxaldehyde, J. Mol. Struct. 1246 (2021) 131204.
[50] S. Menati, R. Azadbakht, H.A. Rudbari, G. Bruno, Synthesis and characterization of four new azo-schiff base and their Nickel (II) complexes, Polyhedron 205 (2021) 115296.
[51] A. Guerraoui, A. Djedouani, E. Jeanneau, A. Boumaza, A. Alsalme, A. Zarrouk, K.S. Salih, I. Warad, Crystal structure and spectral of new hydrazine-pyran–dione derivative: DFT enol↔ hydrazone tautomerization via zwitterionic intermediate, hirshfeld analysis and optical activity studies, J. Mol. Struct. 1220 (2020) 128728.
[52] M. Yahyaoui, A. Bouchama, B. Anak, C. Chiter, A. Djedouani, F. Rabilloud, Synthesis, molecular structure analyses and DFT studies on new asymmetrical azines based Schiff bases, J. Mol. Struct. 1177 (2019) 69–77.
[53] P. Vijaya, K. Sankaran, A combined experimental and DFT study of a novel unsymmetrical azine 2-(4-methoxybenzylidene)-1-(1-(4-isobutylphenyl) ethylidene) hydrazine, Spectrochim. Acta Part A 138 (2015) 460–473.
[54] F. Erdemir, D.B. Celepci, A. Aktaş, Y. Gök, Synthesis, crystal structures, spectral investigations, conformational analysis and DFT studies of N-heterocyclic carbene precursors, J. Mol. Struct. 1204 (2020) 127519.
[55] P.A. Channar, A. Saeed, M.F. Erben, F.A. Larik, S. Riaz, U. Flörke, M. Arshad, Synthesis, conformational studies and NBO analysis of (4-chloro-3, 5-dimethyl-1H-pyrazol-1-yl)(p-tolyl) methanone, J. Mol. Struct. 1191 (2019) 152–157.
[56] X.D. Dexlin, J.D. Tarika, S.M. Kumar, A. Mariappan, T.J. Beaula, Synthesis and DFT computations on structural, electronic and vibrational spectra, RDG analysis and Molecular docking of novel Anti COVID-19 molecule 3, 5 dimethyl pyrazolium 3, 5 dichloro salicylate, J. Mol. Struct. 1246 (2021) 131165.
[57] K. Benbouguerra, N. Chafai, S. Chafaa, Y.I. Touahria, H. Tlidjane, New α-Hydrazinophosphonic acid: synthesis, characterization, DFT study and *in silico* prediction of its potential inhibition of SARS-CoV-2 main protease, J. Mol. Struct. 1239 (2021) 130480.
[58] R.N. Asha, B.R.D. Nayagam, N. Bhuvanesh, Synthesis, molecular docking, and *in silico* ADMET studies of 4-benzyl-1-(2, 4, 6-trimethyl-benzyl)-piperidine: potential Inhibitor of SARS-CoV2, Bioorg. Chem. 112 (2021) 104967.
[59] S. Nallusamy, J. Mannu, C. Ravikumar, K. Angamuthu, B. Nathan, K. Nachimuthu, G. Ramasamy, R. Muthurajan, M. Subbarayalu, K. Neelakandan, Shortlisting phytochemicals exhibiting inhibitory activity against major proteins of SARS-CoV-2 through virtual screening, Res. Square (2020) 1–26.